



This is a repository copy of *Non-linear system identification of solvent-based post-combustion CO2 capture process*.

White Rose Research Online URL for this paper:
<http://eprints.whiterose.ac.uk/138999/>

Version: Accepted Version

Article:

Akinola, T.E., Oko, E., Gu, Y. et al. (2 more authors) (2019) Non-linear system identification of solvent-based post-combustion CO2 capture process. *Fuel*, 239. pp. 1213-1223. ISSN 0016-2361

<https://doi.org/10.1016/j.fuel.2018.11.097>

Article available under the terms of the CC-BY-NC-ND licence
(<https://creativecommons.org/licenses/by-nc-nd/4.0/>).

Reuse

This article is distributed under the terms of the Creative Commons Attribution-NonCommercial-NoDerivs (CC BY-NC-ND) licence. This licence only allows you to download this work and share it with others as long as you credit the authors, but you can't change the article in any way or use it commercially. More information and the full terms of the licence here: <https://creativecommons.org/licenses/>

Takedown

If you consider content in White Rose Research Online to be in breach of UK law, please notify us by emailing eprints@whiterose.ac.uk including the URL of the record and the reason for the withdrawal request.



eprints@whiterose.ac.uk
<https://eprints.whiterose.ac.uk/>

Non-linear system identification of solvent-based post-combustion CO₂ capture process

Toluleke E Akinola^a, Eni Oko^a, Yuanlin Gu^b, Hua-Liang Wei^b, Meihong Wang^{a*}

^a Department of Chemical and Biological Engineering, University of Sheffield, Sheffield. S1 3JD

^b Department of Automatic Control and Systems Engineering, University of Sheffield, Sheffield. S1 3JD

^{a*} Corresponding Author. Tel.: +44 114 222 7160. E-mail address: Meihong.Wang@sheffield.ac.uk

Abstract

Solvent-based post combustion capture (PCC) is a well-developed technology for CO₂ capture from power plants and industry. A reliable model that captures the dynamics of the solvent-based capture process is essential to implement suitable control design. Typically, first principle models are used, however they usually require comprehensive knowledge and deep understanding of the process. System identification approach is adopted to obtain a model that accurately describes the dynamics between key variables in the process. The nonlinear auto-regressive with exogenous (NARX) inputs model is employed to represent the relationship between the input variables and output variables as two Multiple-Input Single-Output (MISO) sub-models. The forward regression with orthogonal least squares (FROLS) algorithm is implemented to select an accurate model structure that best describes the dynamics within the process. The prediction performance of the identified NARX models is promising and shows that the models capture the underlying dynamics of the CO₂ capture process.

Keywords: Solvent-based post-combustion capture; chemical absorption; System Identification; NARX; FROLS-ERR

Highlights

- First principle dynamic model for solvent-based carbon capture process used to generate data
- Solvent-based carbon capture process exhibits a highly nonlinear behaviour
- System Identification of solvent-based CO₂ capture process using NARX model
- Significant model term selection using the FROLS-ERR algorithm
- Developed NARX model accurately predicts CO₂ concentration at absorber outlet and CO₂ lean loading

Abbreviations

BIC	- Bayesian Information Criterion
CCL	- CO ₂ Capture level
CCS	- Carbon Capture and Storage
ERR	- Error Reduction Ratio
FROLS	- Forward Regression with Orthogonal Least Squares
LL	- Lean loading
MIMO	- Multiple Input Multiple Output
MISO	- Multiple Input Single Output
MP	- Mass percentage
MPO	- Multi step-ahead Prediction Output
MSE	- Mean Square Error
NARX	- Nonlinear Auto-regressive with exogenous inputs
NARMAX	- Nonlinear Auto-regressive moving average with exogenous inputs
OSA	- One-Step Ahead Prediction
PCC	- Post Combustion Capture
SISO	- Single Input Single Output

Nomenclature

D	- Dictionary
$F_{CO_2}^{ABS_{in}}$	- Flue gas flowrate at the absorber inlet, kg/s
$F_{CO_2}^{ABS_{out}}$	- Treated gas flowrate at the absorber outlet, kg/s
$n_{CO_2}^{ABS_{in}}$	- CO ₂ mass fraction at the absorber inlet
$n_{CO_2}^{ABS_{out}}$	- CO ₂ mass fraction at the absorber outlet
n_k	- Time delay
n_u	- Maximum lag in the input
n_y	- Maximum lag in the output
$y(t)$	- Response Vector
$x_{ij}(t)$	- Regressors Vector
φ_{ij}	- Parameter Estimate
Φ	- Parameter Vector
n_i	- Number of terms
y_1	- CO ₂ mass percentage at the absorber gas outlet (measured output)
y_2	- CO ₂ lean loading (measured output)
u_1	- Flue gas flowrate (measured input)
u_2	- Lean MEA flowrate (measured input)
u_3	- Reboiler Temperature (measured input)

1 Introduction

1.1 Background

The utilisation of fossil fuels, particularly coal, for electricity generation is recognised as the single largest source of greenhouse gas emissions[1]. CO₂ is the largest anthropogenic greenhouse gas accounting for about three quarters of the global greenhouse gas emitted to the atmosphere[2]. This has resulted in a steady rise in the global average temperature and brought awareness among scientific communities to tackle issues rising from greenhouse gas (GHG) emissions.

Carbon capture and Storage (CCS) is acknowledged to play a major role in the reduction of CO₂ emission from fossil fuel fired power plants. Amongst various CCS technologies, the utilisation of solvent-based post-combustion capture (PCC) process to treat fuel gas from coal fired plant has gained much attention[3]. This is attributed to its suitability to be retrofitted into an existing power plant and its capacity to treat flue gas with low CO₂ partial pressure, giving the solvent-based PCC an edge over other carbon capture technologies[1]. As a result, there has been notable progress in the solvent-based PCC technology development, which has made it the first and only commercial technology that is operational for large-scale coal-fired power plants. Some completed CCS projects include SaskPower Boundary Dam Carbon Capture and Petra Nova Carbon Capture Project[4].

Stringent environmental legislations around the world to reduce CO₂ emissions have prompted the need to deploy new energy sources such as nuclear and renewable energy. This will bring a significant shift in the dominant role of fossil fuel, especially coal, in the energy system and the need for flexible operation of coal fired power plants[5]. The flexible operation of a coal-fired power plant involves the variation of power plant load in accordance to the volatile electricity demand and prices[6]. This result in the fluctuation of the flue gas flowrate and composition to the absorber, as well as steam provided to the reboiler for solvent regeneration, which affects the operation of the capture plant. Thus, the flexible operation of the solvent-based PCC plant (i.e. variation of the capture rate in accordance with electricity demand) is important to cope with the coal-fired power plant operation. Investigation of the capture plant response to disturbances during various flexible operation modes such as start-up, shutdown and load following has gain much attention as well as the need to develop a suitable control strategy for the capture plant to handle these disturbances.

1.2 Literature Review

An accurate and reliable dynamic model is necessary to carry out a comprehensive study on the solvent-based CO₂ capture process. Many studies on dynamic modelling of a solvent-based PCC were carried out on first principle (i.e. mechanistic) models[1,7–12]. Challenges with high computational time when developing a detailed solvent-based PCC model especially when integrated with coal fired power plant and its high level of complexity makes it difficult to implement relevant process control strategies. Thus, simplification of the mechanistic model is required to

reduce the computational time for simulation[13,14]. This has significantly motivated the use of data driven modelling approach and system identification techniques, to represent the solvent-based PCC model. This involves constructing a suitable model that best describes the relationship between the process input and output variables.

In the past, most studies have represented the capture process as a linear model[15–20]. It should be noted that the capture process exhibits highly nonlinear behaviour[21]. The linear model is an approximation of the actual model, which tend to deviate from the actual model when large substantial changes in the input variables enter the carbon capture process[17], especially during flexible operation. Thus, a nonlinear model is essential to capture the actual dynamics within the carbon capture process. Only a few studies have applied non-linear modelling techniques such as neural networks[22–24] and non-linear autoregressive with exogenous input (NARX) model[21] to analyse the CO₂ capture process.

The key steps of system identification include data collection, model structure detection, and model validation[25]. Various studies on system Identification of nonlinear systems have focused on different classes of system, which included volterra series model[26–28], Hammerstein model, Wiener model, Hammerstein-Wiener model[29] and NARMAX model[30,31]. Amongst these classes of nonlinear models, NARMAX model is one of the commonly used representations suitable for a large range of nonlinear systems[30,31]. The key task in system identification using NARMAX and related models centres on model structure detection. The well-known forward regression with orthogonal least squares (FROLS) algorithm has proven to be one of the most efficient approach for nonlinear model structure determination[30,32–34] for the NARMAX model. The FROLS algorithm selects the important model terms one by one, in a stepwise manner, based on their significance, which is measured using a simple but useful index called the error reduction ratio (ERR).

1.3 Aim and Objectives

This paper aims to introduce a data- driven dynamic modelling approach for the solvent-based PCC plant. In this study, the solvent-based CO₂ capture process is represented as NARX models (a special form of NARMAX model). The FROLS algorithm is used to find a most parsimonious (with least parameters) model to represent the relationship between the input variables (flue gas flowrate, lean MEA flowrate and reboiler temperature) and output variables (CO₂ concentration in wt% and CO₂ lean loading).

1.4 Novelty and Structure of Paper

A key novelty of this study is that for the first time, the FROLS algorithm to develop a transparent NARX model that captures the relationship between the input variables and output variables in the carbon capture process. This algorithm enabled us to identify and rank key model terms that contribute to the response variable based on ERR and remove model terms that least contribute to

the system output. The FROLS-ERR algorithm has been extensively used in the literature as an effective system identification technique for various systems[35–38]. To our knowledge, the advantages and potentials of nonlinear system identification techniques, especially dynamic NARMAX models identification with the FROLS-ERR algorithm, have not been well explored for PCC processes.

The paper is structured as follows. Section 2 gives a description of the solvent-based PCC process. The system identification approach using FROLS-ERR algorithm is described in Section 3. Data collection and model identification are presented in Section 4, while Section 5 demonstrates the model performance and discusses the results obtained, statistical analysis as well as the step response analysis. Section 6 provides a brief but useful conclusion and future research consideration.

2 Solvent-based PCC Description

2.1 Solvent-based PCC Process

The solvent-based PCC process mainly consists of absorber and stripper with an aqueous monoethanolamine solution (MEA) as a chemical solvent. The schematic diagram is shown in Fig 1. The absorber typically receives flue gas from the power plants, which flows in from the bottom. The lean solvent is introduced from the top of the absorber and flows counter-currently to strip out CO₂ from the flue gas. Rich CO₂ solvent exits the absorber bottom with the aid of a pump through a heat exchanger into the regenerator while the treated gas leaves the absorber top into the atmosphere. In the regenerator, CO₂ is stripped using heat input from steam extracted from power plants and exits from the top of the regenerator through a condenser to a compression train, where CO₂ gas is compressed and transported via a pipeline for either enhanced oil/gas recovery and, underground storage or various CO₂ utilisation[7]. The regenerated solvent is recycled to the absorber as it flows from the bottom of the regeneration bottom, through the heat exchanger for energy consumption efficiency and water make-up tank to maintain a constant concentration of water. Insights gained from previous studies on the CO₂ capture process was vital in identifying key process variables that are sensitive to the dynamic performance of the capture plant for flexible operation mode[7].

2.2 Selection of Input and Output Variables

In various studies, which includes system identification of the solvent-based capture process, the input and output variables selection were based on the control objectives of the capture process. These objectives are centred on environmental and economic (operational) targets[18].

Key parameters that are sensitive to the control objectives are CO₂ capture level and regeneration efficiency. The CO₂ capture level (CCL) measures the amount of CO₂ captured from the capture plant and can be expressed mathematically as follows:

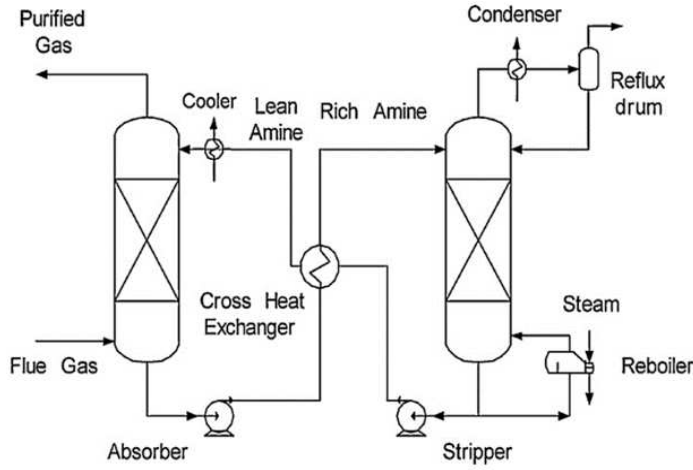


Fig 1 Solvent-based PCC process[7]

$$CCL(\%) = \left(1 - \frac{n_{CO_2}^{ABS_{out}} \times F_{CO_2}^{ABS_{out}}}{n_{CO_2}^{ABS_{in}} \times F_{CO_2}^{ABS_{in}}} \right) \times 100\% \quad (1)$$

where, $n_{CO_2}^{ABS_{out}}$, $F_{CO_2}^{ABS_{out}}$, $n_{CO_2}^{ABS_{in}}$, $F_{CO_2}^{ABS_{in}}$ are CO₂ mass fraction at the absorber gas outlet, flue gas flowrate at the absorber gas outlet, CO₂ mass fraction at the absorber gas inlet and flue gas flowrate at the absorber gas inlet respectively. Thus, the key variable that is sensitive to the CO₂ capture level is the CO₂ mass fraction at the absorber gas outlet ($n_{CO_2}^{ABS_{out}}$), which can be represented as CO₂ mass percentage (CO₂-MP). The regeneration efficiency, which accounts for the bulk of the energy utilisation, is a measure of energy utilised in the regenerator of the capture process. It is acknowledged that the reboiler consumes the most energy and thus dictates the operational cost of the capture process. As stated earlier, steam is extracted from power plants as heat input to the reboiler. The CO₂ lean loading (CO₂-LL) at the lean MEA stream to the absorber is a key process variable that is sensitive to the energy efficiency of the CO₂ capture process. Thus, CO₂-MP and CO₂-LL were selected as the Output variables.

Selection of the input variables was based on key variables (manipulated and disturbance variables) that have significant effect the output variables. Key input variables selected for this study includes flue gas flowrate, lean solvent flowrate and reboiler temperature. Unlike most studies, which used the reboiler duty as an input variable, the reboiler temperature was selected for this study. This is based on study carried out by Lawal et al.[8], in which the reboiler temperature controls the amount of stream drawn off the power plant for regeneration. Thus, the solvent based PCC process was represented as a 3-input and 2-output model.

3 NARX Model

The multivariable Nonlinear Auto-Regressive with eXogenous (NARX) input model, which is a special form of Nonlinear Auto-Regressive Moving Average with eXogenous inputs (NARMAX) model[30,31], is adopted to represent the solvent –based PCC process. The NARX model of Multiple-Input and Single-Output (MISO) systems is described as:

$$y(t) = f(y(t-1), \dots, y(t-n_y), u_1(t), u_1(t-1), \dots, u_1(t-n_u), \dots, u_r(t), u_r(t-1), \dots, u_r(t-n_u)) + e(t) \quad (2)$$

where r is the number of external input signals; $y(t)$, $u_j(t)$, and $e(t)$, with $j = 1, 2, \dots, r$ and $t = 1, 2, \dots, N$ are measured system output, input and unmeasurable noise sequences, respectively; n_y and n_u are the maximum lags in the output and input; $f(\cdot)$ represents a nonlinear function, which is generally unknown but can be approximated using various types of nonlinear forms. Polynomial expansion of $f(\cdot)$ is most commonly used due to its good properties, which include transparency and easy interpretation of the model[30].

The solvent-based CO₂ capture process considered in the present study is a typical MIMO system, involving three inputs (namely, flue gas flowrate, lean MEA flowrate and reboiler temperature) and two outputs (CO₂-MP and CO₂-LL). The MIMO system can be represented as two MISO sub-systems, each of which can be represented using the NARX model (2) as:

$$y_1(t) = f(y_1(t-1), \dots, y_1(t-n_y), u_1(t), u_1(t-1), \dots, u_1(t-n_u), \dots, u_r(t), u_r(t-1), \dots, u_r(t-n_u)) + e_1(t) \quad (3)$$

$$y_2(t) = f(y_2(t-1), \dots, y_2(t-n_y), u_1(t), u_1(t-1), \dots, u_1(t-n_u), \dots, u_r(t), u_r(t-1), \dots, u_r(t-n_u)) + e_2(t) \quad (4)$$

where $r = 3$, u_1 = flue gas flowrate (kg/s), u_2 = Lean MEA flowrate (kg/s), u_3 = Reboiler temperature, and e_1 and e_2 are unmeasurable noise sequences. A graphical illustration of the MISO sub-systems is shown in Fig 2. Each MISO model can be re-arranged into a linear-in-the-parameters form as [39]:

$$y_r(t) = \sum_{j=1}^{M_r} \varphi_{rj} x_{rj}(t) + e_r(t) \quad (5)$$

where $y_r(t)$, $x_{rj}(t)$, φ_{rj} and M_r , with $(r = 1, 2, 3; j = 1, 2, \dots, M_r)$, are the response signal (output), regressors, model parameter and number of model terms. Note that each φ_{rj} is built using lagged input and lagged output variables, such as $y_2(t-1)$, $(y_1(t-1))^2$, $u_2(t-1)u_3(t-4)$, etc. Further details can be found in [39]. The forward regression with orthogonal algorithm (FROLS) is used to select significant model terms for each MISO sub-system.

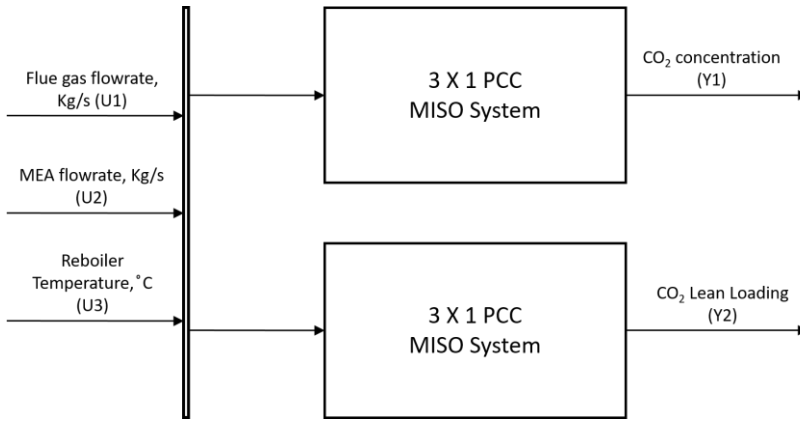


Fig 2 Multiple input single output (MISO) structure of Amine based PCC model

3.1 FROLS

This section discusses the FROLS algorithm and ERR[33,39,40]. Consider the linear in parameters model (5), which can be written in a compact form as:

$$Y = P\Phi + \xi \quad (6)$$

where $Y = [y(1), y(2), \dots, y(N)]^T$ is the measured output vector at N time instants, $P = [P_1, P_2, \dots, P_M]$ is a matrix whose j th column $P_j = [P(1), P(2), \dots, P(N)]^T$ is a vector formed by the j th candidate model term φ_j (as defined in (5)), with $j=1, 2, \dots, M$. $\Phi = [\theta_1, \theta_2, \dots, \theta_M]^T$ is the parameter vector and ξ is the modelling error vector. Note that for convenience of description, the subscript r in (5) is dropped; M is the number of candidate model terms (or the number candidate basis vectors).

The regression matrix P is assumed to be full rank in columns and can be orthogonally decomposed as

$$P = WA \quad (7)$$

where A is an $M \times M$ unit upper triangular matrix and W is an $N \times M$ matrix with orthogonal columns w_1, w_2, \dots, w_M . Equation (6) can be expressed as:

$$Y = (PA^{-1})(A\Phi) + \xi = WG + \xi \quad (8)$$

where $G = [g_1, g_2, \dots, g_M]^T$ is an auxiliary parameter vector, which is calculated from Y and W by means of orthogonality property as follows;

$$g_i = \frac{\langle Y, w_i \rangle}{\langle w_i, w_i \rangle} \quad (9)$$

with $i=1, 2, \dots, M$. The parameter vector Φ is related by the equation $G = A\Phi$. The error reduction ratio (ERR), which provides an effective means for seeking in a subset of significant model term, is calculated as

$$ERR_i = \frac{\langle Y, w_i \rangle}{\langle Y, Y \rangle \langle w_i, w_i \rangle} \times 100\% \quad (10)$$

The significant model terms are selected in a forward-regression pattern. Details on FROLS algorithm procedure for model structure selection can be found in [30,33,39,40].

4 Data Collection and Model Identification

This research obtained dynamic operational data from a dynamically modelled amine- based PCC plant by Lawal et al.[1] using gPROMS and dynamically validated by Biliyok et al.[10]. The simulated data were generated from the model where the time interval for each sample was 60s. All three input variables were simultaneously perturbed for the MISO system representation of the Capture process. Data acquired from the simulation is shown in Fig 3.

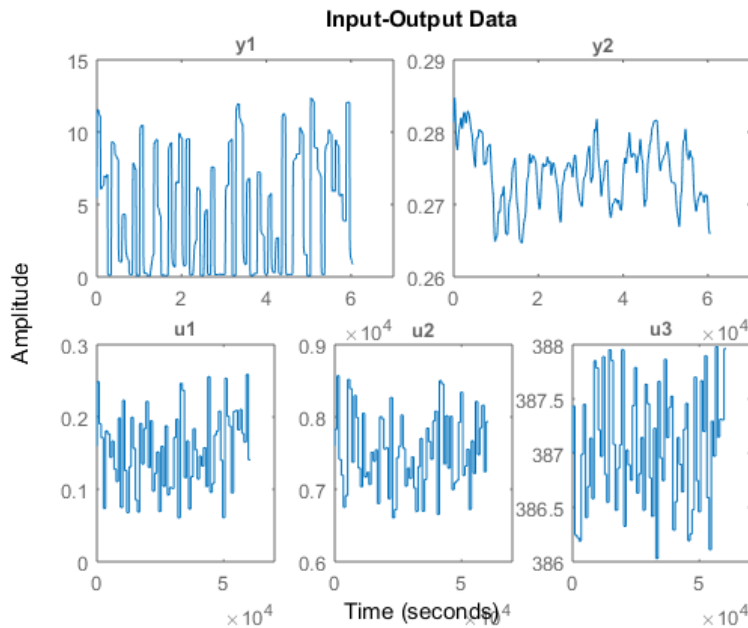


Fig 3 Input – output data obtained from Amine based PCC model developed in gPROMS; u_1 : flue gas flowrate; u_2 = Lean MEA flowrate; u_3 = reboiler temperature; y_1 : CO_2 concentration in wt% at the absorber gas outlet; y_2 = CO_2 lean loading (LL) at the lean solvent stream to the absorber.

Data were carefully observed and outliers were removed. Rigorous pre-treatment was not performed to avoid losing some nonlinear dynamics of the system[41]. The whole data were split into estimation data (75%) and validation (test) data (25%). The estimation (training) data were used for model construction, whereas the test data were used to test the model performance in predicting the CO_2 concentration in wt% (CO_2 mass percentage) at the absorber gas outlet, (y_1) and CO_2 lean loading

(LL) at the lean solvent stream to the absorber, (y_2). The Input variables used for this model development are flue gas flowrate (u_1), lean MEA flowrate (u_2) and reboiler temperature (u_3).

In this study, for both subsystem 1 and subsystem 2, the maximum time lags for the input and output variables were chosen to be $n_y = n_u = 10$ and $n_y = n_u = 4$ respectively. The degree of nonlinearity be 3. The values of n_y and n_u for both sub-systems are large enough to cover the range of potential time lags needed to represent the CO₂ capture process dynamics. In addition, our simulation studies show that a further increase in time lags did not improve the model prediction performance. To show this, following the practice in [33], the values of SERR were calculated from different models with different time lags. In the NARMAX model estimation procedure, SERR (sum of the error reduction ratio) is a measure to determine the maximum time lags for the input and output variables. SERR is an effective index to measure how much (in percentage) of the variance of the output is explained by the lagged input and output variables involved in the model. Fig 4 shows the change of SERR against time lags in both input and output variables. For Sub-system 1, when the time lags $n_y \geq 10$ and $n_u \geq 10$, SERR does not change with the increase of n_y and n_u . Similar, for sub-system 2, SEER becomes unchanged when $n_y \geq 4$ and $n_u \geq 4$. Therefore, we set the maximum time lag for Sub-system 1 as 10 and for Sub-system 2 as 4.

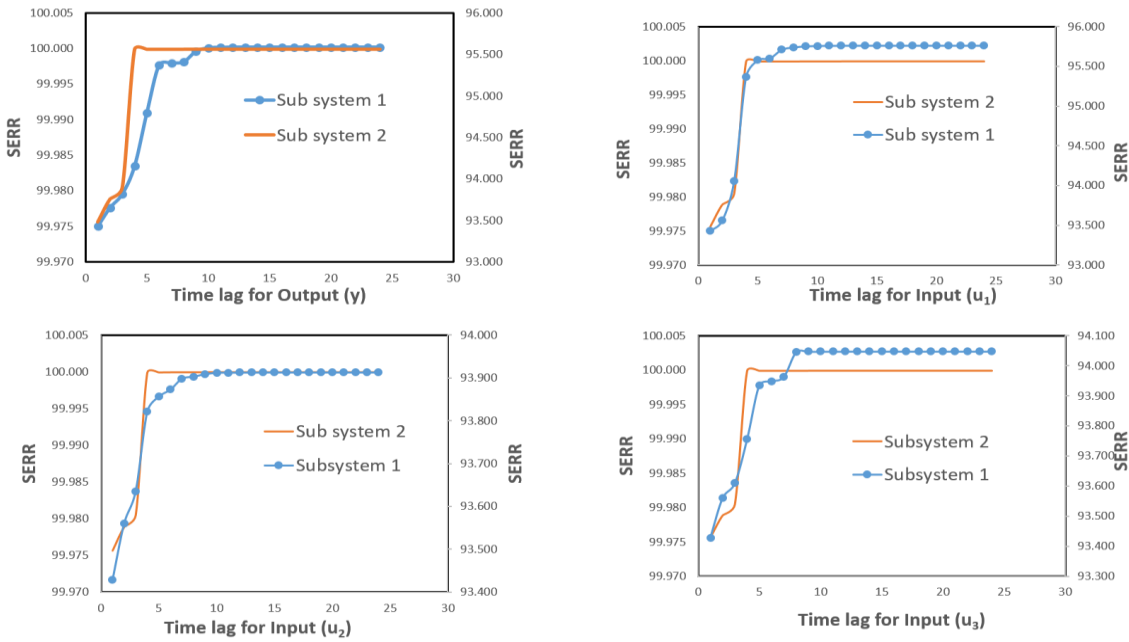


Fig 4 SERR vs Time lags for both input and output variables

Following Wei and Billings [34], the dictionaries of candidate model terms were define as follows:

For subsystem 1;

$$D_0^u = D_{0,10,0,3}, D_0^1 = D_{10,10,0,3}$$

$$D_1^u = D_{0,10,1,3}, D_1^1 = D_{10,10,1,3}$$

For subsystem 2;

$$D_0^u = D_{0,4,0,3}, D_0^1 = D_{4,4,0,3}$$

$$D_1^u = D_{0,4,1,3}, D_1^1 = D_{4,4,1,3}$$

where

$$D_{n_y, n_u, n_k, l} = \{x_1^{i_1}(t) \dots x_l^{i_l}(t) : x_j^{i_j} \in V_{n_y, n_u, n_k}, 1 \leq j \leq l, 0 \leq i_j \leq l, \}$$

$$V_{n_y, n_u, n_k} = \{y(t-1), \dots, y(t-n_y), u(t-n_k), \dots, u(t-n_k-n_u+1)\}.$$

A model term dictionary D is a set consisting of a great number of model building blocks (i.e., candidate model terms)[34]. Here, the two dictionaries D_0^u and D_1^u only contain candidate model terms formed by all input variables alone (i.e., $u_1(t), u_2(t), u_3(t)$ and their lagged versions such as $u_1(t-4), u_2(t-2)$, etc.) but do not include autoregressive model terms such as $y(t-1), \dots, y(t-n_k)$ with $n_k = 0$ and 1 respectively. The other two dictionaries, D_0^1 and D_1^1 , however, contain candidate model terms formed by using all the input variables and all the lagged input and output variables. The main purpose that we separately treat these two group of model (with and without autoregressive variables) is to test whether feedback signals from the system outputs play an obviously important role in explaining the system the system's inherent dynamics.

Using the above 4 dictionaries, a total of 4 models, different model structures, were identified for each sub-system. The model terms were ranked in accordance with their level of significance (measured by ERR index) to the response variable in each sub-model.

The determination of model length (the number of model terms) is important for dynamic modelling and various model selection criteria have been proposed in the literature. In this study, the Bayesian information criterion (BIC) is used to determine the number of model terms[42].

$$BIC(n) = \left[1 + \frac{n \ln(N)}{N-n}\right] MSE(n) \quad (11)$$

where N is the number of samples in the training data set, n is the effective number of model terms, $MSE(n)$ is the mean square error associated with the n -terms model. BIC is commonly used to avoid over-fitting through the penalty factor $n \ln(N)/(N-n)$. The minimum BIC (n) is adopted as the basis for selecting the model length. Thus, the FROLS algorithm stops its iteration at minimum BIC.

Each model identified from the different model term dictionaries were compared based on One-step ahead (OSA) predictions and multi-step (10) ahead predicted outputs (MPO). The models that best predict the system outputs were selected based on the MPO performance criterion.

5 Performance Evaluation

5.1 Sub-model 1

Sub-model 1 represents a MISO system to predict the concentration of CO_2 in wt% at the absorber gas outlet. Tables 1-4 gives details of various model structures selected for each model term

candidate dictionary ($D_1^u, D_1^1, D_0^u, D_0^1$) using FROLS algorithm along with the parameter estimates and BIC. It can be deduced from the sum of error reduction ratio (SERR), that the list of model terms selected from dictionary D_0^1 gives the best explanation (99.90%) of the response variable variation compared to the identified model developed from other dictionaries (see Table 4) .

Furthermore, comparisons of the identified models obtained from the different model dictionaries were carried out to assess the predictive ability of the models. Each of the models was applied to the test data for concentration of CO₂ in wt% at absorber gas outlet. The associated one-step ahead predictions and multi-step (10) ahead predicted outputs are calculated and shown in Figs. 5-8, where the solid line represents the original measurements and the dashed blue and red lines are for the one-step ahead prediction and multi-step (10) ahead predicted output, respectively.

As shown in Fig 5 and Fig 7, models M_1^u (see Table 1) and model M_0^u (see Table 3) gave similar MPO and OSA performance, this is because these models only use exogenous inputs ($u(t-1), \dots, u_r(t-1), \dots, u_r(t-n)$) and do not use any autoregressive model terms ($y(t-1), \dots, y(t-n)$). For models that only use exogenous inputs (without using autoregressive terms), their MPO and OSA predictions are always the same. Models M_1^1 and M_0^1 (see Table 2 and Table 3 respectively), however, involve both the autoregressive variables and the exogenous input variables. Comparing Figs 5-8, it can be seen that model M_0^1 gave the best prediction performance (Fig 8), indicating that M_0^1 contains the appropriate model terms that capture the dynamics of the system. For M_1^1 , there was disparity between the MPO and OSA prediction performances, this is because M_1^1 does not contain the most appropriate model terms that can well capture the system dynamics. For such a deficient model, its MPO performance will usually deteriorate because the accumulative error can be significantly augmented through an iterative computation procedure when updating the system output values. The OSA performance of such a deficient model, however, normally does not suffer from any error accumulation and propagation. The discrepancy between MPO and OSA shown in Fig 6 (formally Fig 5) is mainly caused by the error propagation and augmentation due to the deficiency of the model. MPO is often used to test the validity of a dynamic model that cannot be easily revealed by OSA.

The variance accounted for (VAF), also called the prediction efficiency (PE), of the identified models are shown in Table 5. VAF (and PE) is calculated as:

$$VAF = \left[1 - \frac{\text{var}(y_{measure} - y_{predict})}{\text{var}(y_{measure})} \right] \times 100\% \quad (12)$$

where $y_{measure}$ is the measured output of the test data and $y_{predict}$ is the one-step ahead prediction/ multi step-ahead prediction output. Among the 4 models, $M_1^u, M_1^1, M_0^u, M_0^1$ (obtained based upon

the 4 dictionaries, $D_1^u, D_1^1, D_0^u, D_0^1$, It can be seen from Table 5 that model M_0^1 gave the best performance compared to the other 3 models with a prediction efficiency of 98.93% and 98.55% in terms of OSA and MPO respectively (see Fig.8). This indicates that the underlying dynamics between the inputs and the output (concentration of CO₂ in wt% at the absorber gas outlet) is captured by model M_0^1 [23]. Thus, model M_0^1 was selected to represent sub-system 1. From Table 4, the system model can be written as:

$$y_1(t) = 3.66 \times 10^1 y_1(t-1).u_1(t) + 2.76 \times 10^{-1} y_1(t-1)^2.u_1(t-1) + \dots + 2.11 \times 10^{-2} u_1(t-1).u_1(t-2).u_2(t). \quad (13)$$

Table 1 Identified model (M_1^u) structures from D_1^u for sub-model 1 using FROLS algorithm

Model Terms	Parameter Estimates	ERR (%)	BIC
$u_1(t-1)^2$	1.08E+04	8.70E+01	4.04E+00
$u_1(t-1).u_2(t-1)^2$	-6.81E+02	3.97E+00	2.84E+00
$u_1(t-1)^3$	-5.85E+03	1.47E+00	2.40E+00
$u_1(t-1)^2.u_3(t-10)$	-2.61E+01	3.55E-01	2.31E+00
$u_1(t-10)^2$	-2.65E+02	1.37E-01	2.28E+00
$u_1(t-10)^2.u_2(t-1)$	1.35E+02	8.97E-02	2.27E+00
$u_2(t-1)^2.u_2(t-10)$	-8.58E+00	1.04E-01	2.26E+00
$u_1(t-1)^2.u_2(t-1)$	3.01E+03	2.16E-01	2.21E+00
$u_2(t-1)^3$	4.42E+01	6.92E-01	2.00E+00
$u_1(t-1)^2.u_1(t-10)$	-1.49E+02	8.13E-02	1.98E+00
$u_1(t-10)^2.u_2(t-10)$	2.18E+02	4.96E-02	1.98E+00

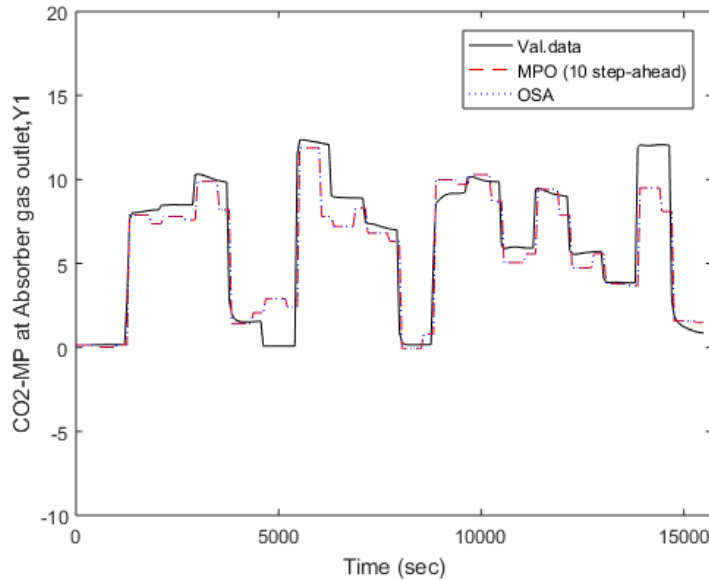


Fig 5 A comparison of the model predictions (OSA and MPO) and measurements over the test data for sub-system 1 using model M_1^u (Table 1).

Table 2 Identified model (M_1^1) structures from D_1^1 for sub-model 1 using FROLS algorithm

Model Terms	Parameter Estimates	ERR (%)	BIC
$y_1(t-1)$	8.02E-01	9.34E+01	2.05E+00
$y_1(t-1) \cdot y_1(t-10) \cdot u_3(t-10)$	-1.99E-04	2.87E-01	1.98E+00
$u_1(t-1)^2$	4.99E+03	1.61E-01	1.95E+00
$u_1(t-1) \cdot u_1(t-2) \cdot u_2(t-1)$	-9.91E+01	2.27E-01	1.89E+00
$u_1(t-1)^2 \cdot u_3(t-10)$	-1.26E+01	1.01E-01	1.88E+00
$y_1(t-1) \cdot y_1(t-10) \cdot u_2(t-1)$	1.21E-01	4.71E-02	1.88E+00
$y_1(t-10) \cdot u_1(t-1)^2$	-4.78E+00	6.24E-02	1.88E+00

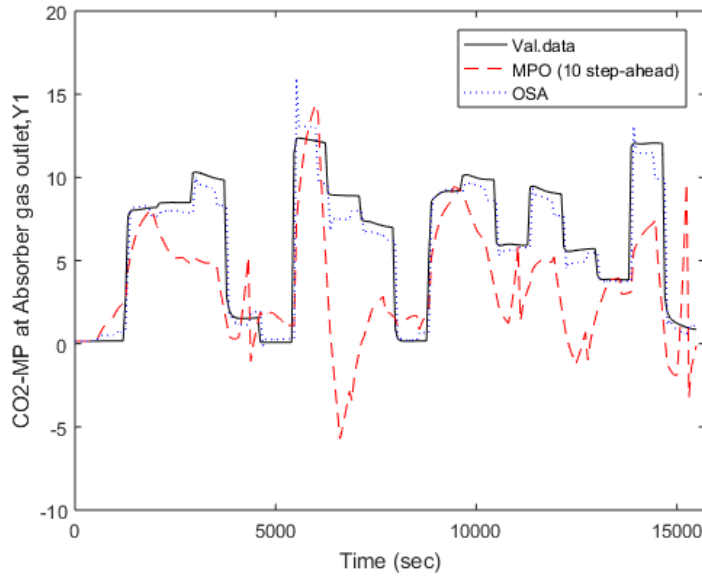


Fig 6 A comparison of the model predictions (OSA and MPO) and measurements over the test data for sub-system 1 using model M_1^1 (Table 2)

Table 3 Identified model (M_0^u) structures from D_0^u for sub-model 1 using FROLS algorithm

Model Terms	Parameter Estimates	ERR (%)	BIC
$u_1(t)^3$	-3.40E+02	9.14E+01	2.68E+00
$u_1(t) \cdot u_1(t-1)$	7.66E+03	8.28E-01	2.44E+00
$u_1(t-1) \cdot u_2(t)^2$	-5.27E+02	3.81E+00	1.26E+00
$u_1(t)^2 \cdot u_1(t-1)$	-2.07E+03	1.51E+00	7.87E-01
$u_1(t) \cdot u_3(t-10)^2$	-5.57E-01	2.71E-01	7.07E-01
$u_2(t)^3$	5.27E+01	3.84E-01	5.88E-01
$u_1(t) \cdot u_3(t-1)$	-3.80E+02	1.55E-01	5.43E-01
$u_1(t) \cdot u_1(t-1) \cdot u_2(t)$	2.11E+03	4.89E-02	5.31E-01
$u_1(t) \cdot u_2(t) \cdot u_3(t-2)$	-6.17E-01	5.66E-01	3.48E-01
$u_1(t)^2 \cdot u_2(t)$	7.95E+02	2.18E-01	2.77E-01
$u_1(t-1)^3$	-1.52E+03	7.86E-02	2.53E-01
$u_1(t-1)^2 \cdot u_2(t)$	1.21E+03	2.80E-02	2.46E-01
$u_1(t) \cdot u_1(t-1) \cdot u_3(t-1)$	-8.04E+01	3.23E-02	2.37E-01
$u_2(t-2) \cdot u_3(t-6)$	1.09E-01	2.63E-02	2.30E-01
$u_1(t) \cdot u_1(t-1)^2$	-2.59E+03	2.36E-02	2.23E-01
$u_1(t-2) \cdot u_2(t-2)^2$	3.71E+01	2.55E-02	2.16E-01
$u_1(t-2) \cdot u_2(t) \cdot u_2(t)$	-2.55E+00	1.86E-02	2.11E-01
$u_2(t)^2 \cdot u_3(t-2)$	5.41E-03	2.70E-02	2.03E-01
$u_1(t) \cdot u_3(t-1) \cdot u_3(t-10)$	1.05E+00	1.13E-02	2.01E-01

Model Terms	Parameter Estimates	ERR (%)	BIC
$u_2(t-2) \cdot u_3(t-1) \cdot u_3(t-6)$	-3.96E-04	1.46E-02	1.97E-01
$u_2(t) \cdot u_2(t-2) \cdot u_3(t-10)$	2.47E+00	1.02E-02	1.95E-01
$u_1(t)$	7.34E+04	9.19E-03	1.93E-01
$u_1(t)^2 \cdot u_2(t-9)$	2.22E+02	8.53E-03	1.91E-01
$u_1(t-1) \cdot u_2(t) \cdot u_2(t-9)$	1.50E+02	1.66E-02	1.87E-01
$u_1(t) \cdot u_2(t-9) \cdot u_3(t-5)$	-5.22E-01	8.11E-03	1.85E-01
$u_1(t-2) \cdot u_2(t-1) \cdot u_3(t-1)$	-3.96E+00	7.47E-03	1.84E-01
$u_1(t-2) \cdot u_2(t-1) \cdot u_3(t-10)$	3.90E+00	1.51E-02	1.79E-01
$u_2(t-9)^3$	3.56E+00	5.97E-03	1.78E-01
$u_1(t) \cdot u_1(t-1) \cdot u_3(t-10)$	6.07E+01	4.49E-03	1.78E-01
$u_2(t) \cdot u_2(t-2) \cdot u_3(t-1)$	-2.45E+00	3.33E-02	1.66E-01

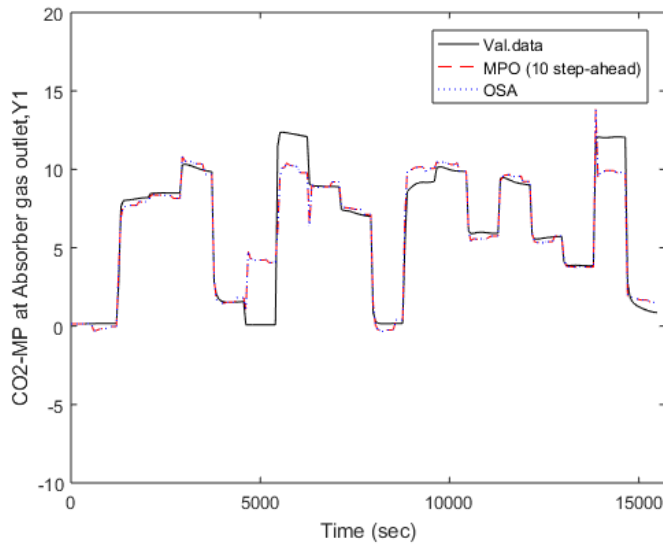


Fig 7 A comparison of the model predictions (OSA and MPO) and measurements over the test data for sub-system 1 using model M_0^u (Table 3)

Table 4 Identified model (M_0^1) structures from D_0^1 for sub-model 1 using FROLS algorithm

Model Terms	Parameter Estimates	ERR (%)	BIC
$y_1(t-1) \cdot u_1(t)$	3.66E+01	9.41E+01	1.84E+00
$y_1(t-1)^2 \cdot u_1(t-1)$	2.76E-01	2.94E+00	9.38E-01
$u_1(t)^3$	-7.79E+02	6.37E-01	7.45E-01
$y_1(t-1) \cdot u_1(t) \cdot u_2(t)$	6.81E+00	1.05E+00	4.18E-01
$u_1(t)^2 \cdot u_1(t-1)$	1.01E+03	4.15E-01	2.88E-01
$y_1(t-1)^2 \cdot u_1(t)$	-8.99E-01	1.41E-01	2.45E-01
$u_1(t-1)^2 \cdot u_2(t)$	-9.52E+02	1.67E-01	1.93E-01
$y_1(t-1) \cdot u_1(t) \cdot u_3(t-10)$	-4.17E-02	6.68E-02	1.73E-01
$y_1(t-1) \cdot u_1(t)^2$	-4.74E+01	4.43E-02	1.59E-01
$y_1(t-1) \cdot u_2(t)^2$	-3.95E+00	4.60E-02	1.45E-01
$u_1(t)^2 \cdot u_2(t)$	-6.36E+02	2.91E-02	1.37E-01
$u_1(t-1) \cdot u_2(t) \cdot u_2(t-2)$	2.10E+02	7.67E-02	1.12E-01
$y_1(t-1)^3$	7.57E-03	3.21E-02	1.02E-01
$u_1(t)^2$	1.28E+04	1.78E-02	9.62E-02
$u_1(t) \cdot u_2(t-2) \cdot u_3(t-4)$	-4.07E-01	2.27E-02	8.91E-02
$u_1(t) \cdot u_1(t-1) \cdot u_3(t-3)$	-2.04E+00	1.44E-02	8.48E-02

Model Terms	Parameter Estimates	ERR (%)	BIC
$u_1(t)$	1.68E+01	4.29E-02	7.02E-02
$u_2(t-2) \cdot u_3(t-7)^2$	-1.21E-05	2.03E-02	6.35E-02
$y_1(t-1)^2 \cdot u_1(t-2)$	1.81E-01	7.35E-03	6.13E-02
$u_1(t)^2 \cdot u_3(t-6)$	-3.00E+01	6.71E-03	5.94E-02
$u_1(t-1) \cdot u_1(t-2)$	-1.15E+04	3.49E-03	5.86E-02
$u_1(t-1) \cdot u_1(t-2) \cdot u_3(t-6)$	2.91E+01	1.09E-02	5.50E-02
$u_1(t-2) \cdot u_2(t-2) \cdot u_2(t-3)$	1.03E+01	4.29E-03	5.38E-02
$y_1(t-1) \cdot u_2(t-1)$	2.25E+00	6.58E-03	5.18E-02
$y_1(t-1) \cdot u_1(t-1) \cdot u_3(t-2)$	-5.27E-02	8.61E-03	4.89E-02
$u_1(t-1)^2 \cdot u_2(t-1)$	-1.61E+02	7.07E-03	4.66E-02
$u_1(t) \cdot u_1(t-1)^2$	4.10E+03	5.54E-03	4.49E-02
$y_1(t-1) \cdot u_1(t-1) \cdot u_2(t)$	2.41E+01	6.73E-03	4.26E-02
$y_1(t-1) \cdot u_1(t) \cdot u_1(t-1)$	-4.57E+01	3.67E-03	4.15E-02
$u_1(t-1) \cdot u_3(t-1)^2$	3.20E-04	2.73E-03	4.07E-02
$u_1(t-1) \cdot u_1(t-2) \cdot u_2(t)$	2.11E+02	3.49E-03	3.97E-02

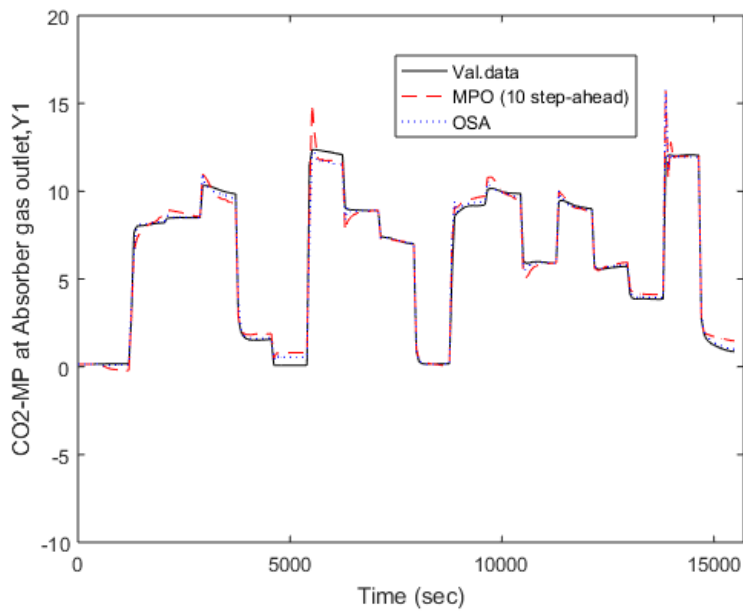


Fig 8 A comparison of the model predictions (OSA and MPO) and measurements over the test data for sub-system 1 using model M_0^1 (Table 4)

Table 5 VAF (and PE) for the Identified sub-model 1 (OSA and MPO)

Identified Models	OSA (%VAF)	MPO (%VAF)
M_1^u	84.8116	84.8116
M_1^1	89.0702	26.4270
M_0^u	90.2407	90.2407
M_0^1	98.9329	98.5494

5.2 Sub-model 2

The details of the models for sub-system 2, obtained from each model term dictionary based on FROLS algorithm, are summarized in Tables 6-9. OSA predictions and the multi-step (10) prediction outputs (MPO) generated by these models, together with the true values (i.e. the system output measurements as test data), are shown in Figs. 9-12, respectively. Also, the prediction efficiency for each identified model is tabulated in Table 10.

It was observed from Table 10 that M_1^1 (obtained from D_1^1) out-performed the other 3 models with a prediction efficiency of 99.996% and 99.295% based on OSA prediction and MPO (see Fig.10) and was selected as a suitable model to predict the CO₂ loading at lean solvent stream to the absorber. Thus, from Table 7, the model should be written as:

$$y_2(t) = -9.626 \times 10^{-1} y_2(t-1) - 3.046 y_2(t-2) + 8.088 y_2(t-3) + \dots - 8.592 \times 10^{-3} u_1(t-4)^3 \quad (14)$$

Table 6 Identified model (M_1^u) structures from D_1^u for sub-model 2 using FROLS algorithm

Model Terms	Parameter Estimates	ERR (%)	BIC
Constant	2.72E+05	9.998E+01	1.822E-05
$u_3(t-4)^3$	-4.69E-03	9.498E-03	1.110E-05
$u_1(t-3) \cdot u_2(t-2) \cdot u_2(t-3)$	8.33E-02	3.316E-03	8.631E-06
$u_1(t-3) \cdot u_2(t-4)$	-1.54E+01	1.191E-04	8.614E-06
$u_1(t-3) \cdot u_2(t-4) \cdot u_3(t-4)$	3.96E-02	3.994E-04	8.374E-06
$u_2(t-2) \cdot u_3(t-4)^2$	-3.92E-06	1.887E-04	8.297E-06
$u_2(t-2)^2 \cdot u_3(t-1)$	1.00E-03	8.709E-04	7.671E-06
$U_1(t-1) \cdot u_1(t-2) \cdot u_1(t-4)$	9.22E-02	1.741E-04	7.596E-06
$U_3(t-4)$	-2.11E+03	1.290E-04	7.555E-06
$u_3(t-4)^2$	5.45E+00	5.410E-04	7.376E-06

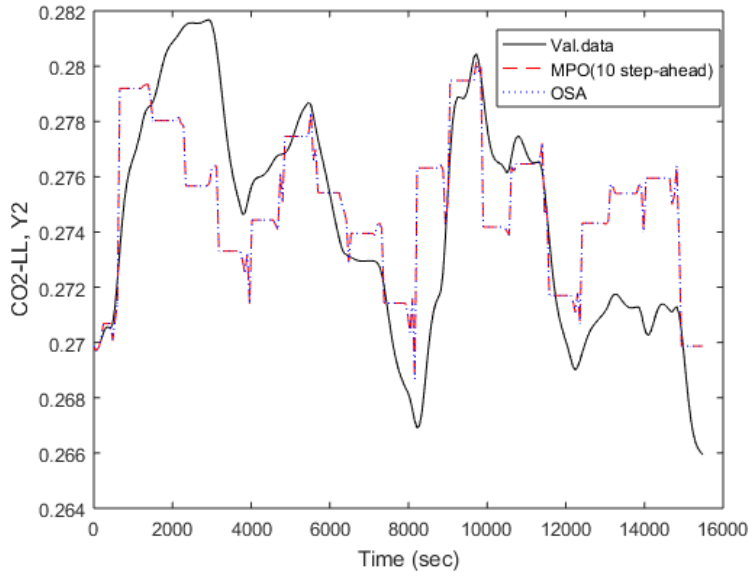


Fig 9 A comparison of the model predictions (OSA and MPO) and measurements over the test data for sub-system 1 using model M_1^u (Table 6)

Table 7 Identified model (M_1^1) structures from D_1^1 for sub-model 2 using FROLS algorithm

Model Terms	Parameter Estimates	ERR (%)	BIC
$y_2(t-1)$	-9.62619E-01	9.99998E+01	1.81E-07
$y_2(t-2)$	-3.04635E+00	2.11626E-04	2.51E-08
$y_2(t-3)$	8.08849E+00	2.41450E-05	8.01E-09
$y_2(t-4)$	-3.00770E+00	3.62552E-06	5.21E-09
$y_2(t-4) \cdot u_3(t-1)^2$	1.83104E-05	6.11699E-07	4.78E-09
$u_3(t-2) \cdot u_3(t-3)^2$	3.43543E-11	9.60331E-07	4.06E-09
$u_1(t-1) \cdot u_2(t-1)^2$	2.76765E-02	3.21983E-07	3.83E-09
$u_1(t-1) \cdot u_2(t-1) \cdot u_2(t-2)$	-4.35975E-02	2.56125E-06	1.79E-09
$u_1(t-4) \cdot u_2(t-3)^2$	1.16669E-03	9.25644E-07	1.86957E-07
$u_1(t-4) \cdot u_2(t-1) \cdot u_2(t-4)$	9.45817E-03	2.21528E-07	2.64208E-08
$u_1(t-1) \cdot u_2(t-2)^2$	1.87578E-02	8.99773E-08	7.98600E-09
$u_1(t-4) \cdot u_2(t-2)^2$	-1.41110E-03	5.48114E-08	5.22828E-09
$u_1(t-3) \cdot u_2(t-4)^2$	-3.37124E-03	4.27371E-08	4.79243E-09
$y_2(t-1) \cdot u_3(t-1)^2$	2.51387E-05	3.99636E-08	4.07181E-09
$u_1(t-2) \cdot u_2(t-1)^2$	-4.56392E-05	4.31311E-08	3.84904E-09
$y_2(t-3) \cdot u_3(t-1)^2$	-4.39772E-05	1.61118E-08	1.81491E-09
$u_1(t-4) \cdot u_2(t-2) \cdot u_2(t-3)$	-8.97025E-03	9.24157E-09	1.07697E-09
$u_1(t-2) \cdot u_1(t-3) \cdot u_2(t-4)$	1.18365E-02	6.71486E-09	9.04236E-10
$u_1(t-1) \cdot u_1(t-2) \cdot u_2(t-3)$	-7.73954E-03	1.63813E-07	8.37345E-10
$u_1(t-4)^3$	-8.59219E-03	4.49587E-08	7.98578E-10

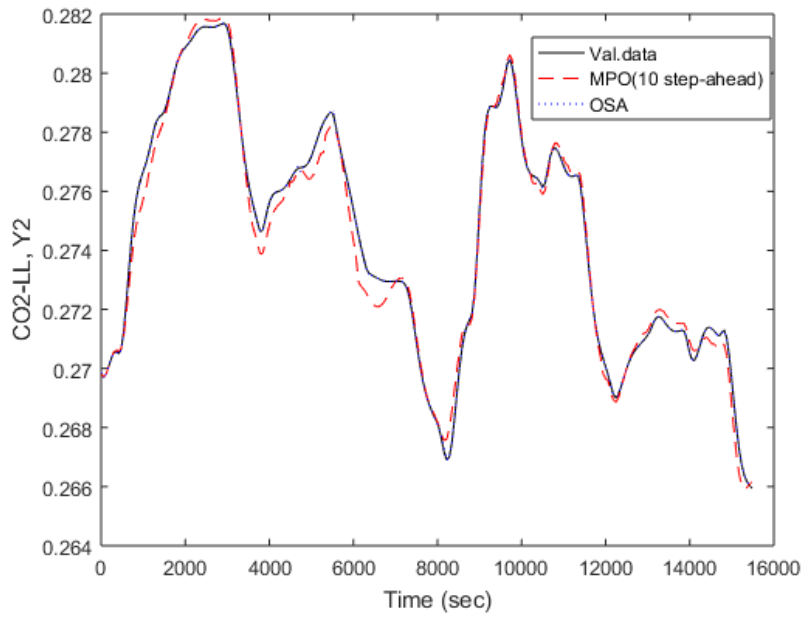


Fig 10 A comparison of the model predictions (OSA and MPO) and measurements over the test data for sub-system 1 using model M_1^1 (Table 7).

Table 8 Identified model (M_0^u) structures from D_0^u for sub-model 2 using FROLS algorithm

Model Terms	Parameter Estimates	ERR (%)	BIC
Constant	2.69E+05	9.9976E+01	1.82E-05
$u_3(t-4)^3$	-4.64E-03	9.4979E-03	1.11E-05
$u_1(t-4) \cdot u_2(t-2) \cdot u_2(t-3)$	1.07E-01	3.3155E-03	8.63E-06
$u_1(t-3) \cdot u_2(t-3)$	-1.52E+01	1.1112E-04	8.62E-06
$u_2(t-2)$	-5.96E-01	4.3718E-04	8.35E-06
$u_2(t-2)^2 \cdot u_3(t-1)$	1.01E-03	7.1404E-04	7.86E-06
$u_1(t-3) \cdot u_2(t-3) \cdot u_3(t-4)$	3.91E-02	3.7740E-04	7.62E-06
$u_1(t) \cdot u_1(t-2) \cdot u_1(t-3)$	1.08E-01	1.5916E-04	7.56E-06
$u_3(t-4)$	-2.09E+03	1.2342E-04	7.52E-06
$u_3(t-1)^2$	5.39E+00	5.3801E-04	7.34E-06

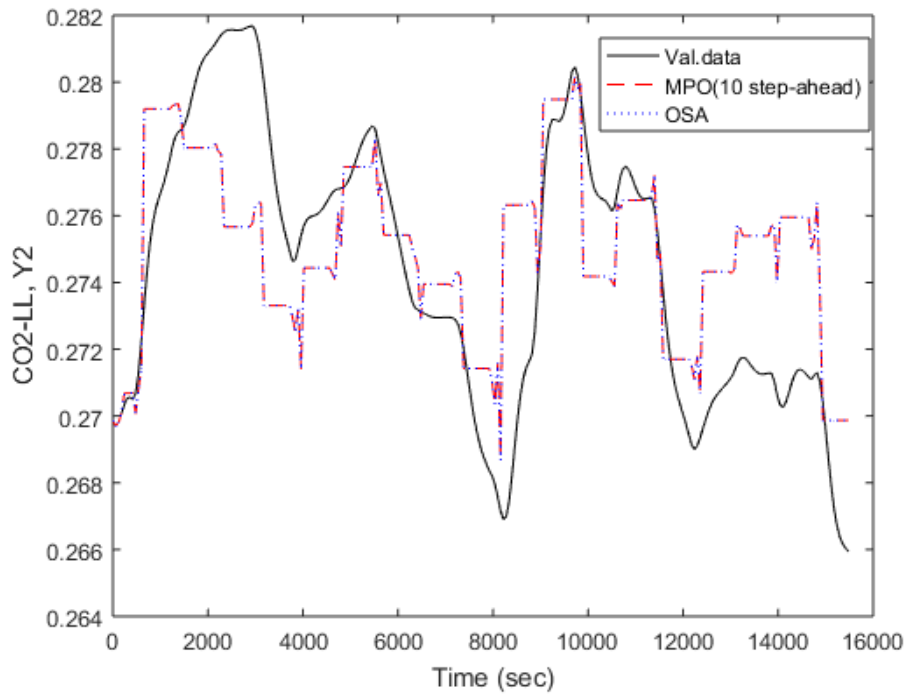


Fig 11 A comparison of the model predictions (OSA and MPO) and measurements over the test data for sub-system 1 using model M_0^u (Table 8)

Table 9 Identified model (M_0^1) structures from D_0^1 for sub-model 2 using FROLS algorithm

Model Terms	Parameter Estimates	ERR (%)	BIC
$y_2(t-1)$	-2.16623E+00	9.99998E+01	1.86957E-07
$y_2(t-2)$	-3.02998E+00	2.11626E-04	2.64208E-08
$y_2(t-3)$	1.12774E+01	2.41450E-05	7.98600E-09
$y_2(t-4)$	-5.00591E+00	3.62552E-06	5.22828E-09
$y_2(t-4) \cdot u_3(t-1)^2$	3.15751E-05	6.11699E-07	4.79243E-09
$u_3(t-2)^2 \cdot u_3(t-3)$	3.60624E-11	9.60331E-07	4.07181E-09
$u_1(t-1) \cdot u_2(t)^2$	3.31495E-03	3.39815E-07	3.83477E-09
$u_1(t-3) \cdot u_2(t-3)^2$	-9.38304E-03	1.19311E-06	2.90460E-09
$u_1(t-3) \cdot u_2(t-1)^2$	2.35993E-02	1.27838E-06	1.88882E-09
$u_1(t-3) \cdot u_2(t-1) \cdot u_2(t-2)$	-2.78876E-02	8.30813E-07	1.22289E-09
$u_1(t-3) \cdot u_2(t-2) \cdot u_2(t-3)$	1.00523E-02	9.42003E-08	1.15517E-09
$y_2(t-1) \cdot u_3(t-1)^2$	3.30630E-05	4.65104E-08	1.12598E-09
$u_1(t-2) \cdot u_1(t-3) \cdot u_2(t-3)$	4.74655E-02	4.29128E-08	1.09919E-09
$u_1(t-1) \cdot u_1(t-2) \cdot u_2(t)$	1.67865E-02	1.21565E-07	1.00512E-09
$u_1(t-2) \cdot u_1(t-3) \cdot u_2(t)$	-3.82933E-02	8.89176E-08	9.37308E-10
$u_1(t-1) \cdot u_1(t-2) \cdot u_2(t-3)$	-2.29989E-02	4.80071E-08	9.03550E-10
$u_1(t-1)^3$	-4.88360E-03	2.64740E-08	8.87858E-10
$y_2(t-3) \cdot u_3(t-1)^2$	-6.51919E-05	2.60335E-08	8.72339E-10

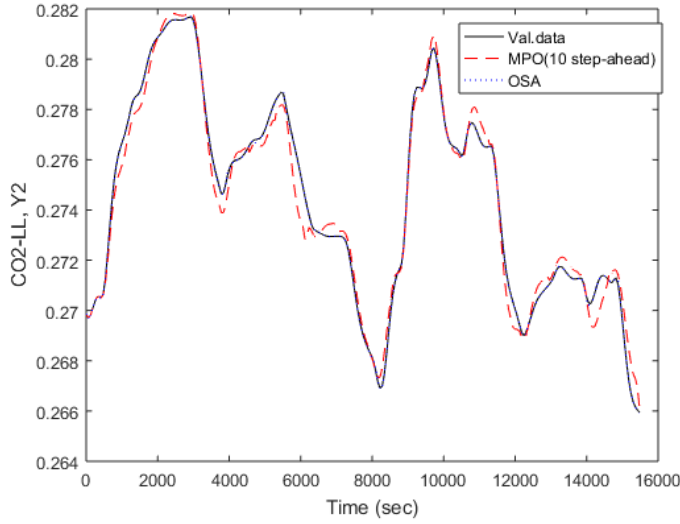


Fig 12 . A comparison of the model predictions (OSA and MPO) and measurements over the test data for sub-system 1 using model M_0^1 (Table 9).

Table 10 VAF (and PE) for the Identified sub-model 2 (OSA and MPO)

Identified Models	OSA (%VAF)	MPO (%VAF)
M_1^u	42.2227	42.2227
M_1^1	99.9971	98.8362
M_0^u	42.2227	42.2227
M_0^1	99.9941	98.0601

5.3 Statistical Analysis

Statistical analysis was carryout on the suitable NARX models obtained using FROLS algorithm to represent the underlying dynamics between key variables in the solvent-based CO₂ capture plant. Table 11 shows the values of R, R² and adjusted R² of the identified models. R, which is the multiple correlation coefficient, is a measure of how much the combination of model terms in each identified model correlates with the respective output variables. The R² represents the portion of variance in the response variable that is explained by the combination of model terms, while the adjusted R² is a measure of the accuracy of a model across different samples. R, R² and adjusted R² are calculated as follows:

$$R = \frac{N \sum y_{measure} y_{predict} - \sum y_{measure} \sum y_{predict}}{\sqrt{N \sum y_{measure}^2 - (\sum y_{measure})^2} \sqrt{N \sum y_{predict}^2 - (\sum y_{predict})^2}} \quad (15)$$

$$R^2 = 1 - \frac{SSE}{SST} \quad (16)$$

$$R_{adj}^2 = 1 - \left(\frac{N-1}{N-n} \right) \frac{SSE}{SST} \quad (17)$$

where $y_{measure}$ is the measured output; $y_{predict}$ is the multi-step ahead prediction; SSE is the sum of squares error; SST is the total sum of squares; N is the number of observations and n is the number of terms. The R-value for sub-model1 (1.000) and sub-model 2 (1.000) indicates that the combination of model terms in each identified model are highly correlated with the response variables. The R^2 value signifies that model 1 can explain 99.80% of the variation in the concentration of CO₂ in wt% at the absorber gas outlet and model 2 can explain 99.58% of the variation in CO₂ lean loading at the lean solvent stream to the absorber. The values of adjusted R^2 indicates that the identified NARX models has high accuracy of prediction even across different samples.

Table 11 Statistical performance of the identified Narx Model

Identified Model	R	R^2	R^2_{adj}
Sub-model 1	1.0000	0.9980	0.9980
Sub-model 2	1.0000	0.9958	0.9957

6 Conclusion and Recommendations

In this study, a parsimonious polynomial NARX model was developed to predict the dynamic responses of an amine based PCC plant (3-inputs and 2-outputs) using the FROLS-ERR algorithm. The amine based PCC plant was represented as two MISO sub-systems (3-inputs and 2-outputs). The FROLS-ERR algorithm proved to be a powerful tool in selecting the most significant model terms for representing and predicting the response variables (CO₂-MP and CO₂-LL). These model terms were ranked based on ERR. This gives a simple and transparent mathematical representation of the systems where we can clearly know how the system outputs depend on the variables and their interactions.

Identified models obtained from the different model term dictionaries were compared, in which the best model was selected based on the performance of multi-step ahead prediction output (MPO) and one-step ahead prediction (OSA). M_0^1 and M_1^1 gave the best performances based on the prediction efficiency of both OSA and MPO for both subsystem-1 and subsystem-2. Further statistical analysis indicated that the identified NARX models captures the underlying dynamics of the sub-systems. Multivariable control analysis of the capture process using the identified NARX models will be studied in the future.

Acknowledgment

The authors acknowledge financial support from EU FP7 Marie Curie International Research Staff Exchange Scheme (IRSES) (Ref: PIRSES-GA-2013-612230); The Engineering and Physical Sciences Research Council (EPSRC) under Grant EP/I011056/1; and Platform Grant EP/H00453X/1.

Reference

- [1] Lawal A, Wang M, Stephenson P, Koumpouras G, Yeung H. Dynamic modelling and analysis of post-combustion CO₂ chemical absorption process for coal-fired power plants. *Fuel* 2010;89:2791–801.
- [2] Huaman RNE, Jun TX. Energy related CO₂ emissions and the progress on CCS projects: a review. *Renew Sustain Energy Rev* 2014;31:368–85.
- [3] Wang M, Lawal A, Stephenson P, Sidders J, Ramshaw C. Post-combustion CO₂ capture with chemical absorption: a state-of-the-art review. *Chem Eng Res Des* 2011;89:1609–24.
- [4] Mumford KA, Wu Y, Smith KH, Stevens GW. Review of solvent based carbon-dioxide capture technologies. *Front Chem Sci Eng* 2015;9:125–41.
- [5] Mac Dowell N, Staffell I. The role of flexible CCS in the UK's future energy system. *Int J Greenh Gas Control* 2015.
- [6] Bui M, Gunawan I, Verheyen V, Feron P, Meuleman E, Adeloju S. Dynamic modelling and optimisation of flexible operation in post-combustion CO₂ capture plants—A review. *Comput Chem Eng* 2014;61:245–65.
- [7] Lawal A, Wang M, Stephenson P, Yeung H. Dynamic modelling of CO₂ absorption for post combustion capture in coal-fired power plants. *Fuel* 2009;88:2455–62.
- [8] Lawal A, Wang M, Stephenson P, Obi O. Demonstrating full-scale post-combustion CO₂ capture for coal-fired power plants through dynamic modelling and simulation. *Fuel* 2012;101:115–28.
- [9] Biliyok C, Lawal A, Wang M, Seibert F. Dynamic Validation of Model for Post-Combustion Chemical Absorption CO₂ Capture Plant. *Comput Aided Chem Eng* 2012;30:807–11.
- [10] Biliyok C, Lawal A, Wang M, Seibert F. Dynamic modelling, validation and analysis of post-combustion chemical absorption CO₂ capture plant. *Int J Greenh Gas Control* 2012;9:428–45.
- [11] Mac Dowell N, Samsatli NJ, Shah N. Dynamic modelling and analysis of an amine-based post-combustion CO₂ capture absorption column. *Int J Greenh Gas Control* 2013;12:247–58.
- [12] Mac Dowell N, Shah N. Dynamic modelling and analysis of a coal-fired power plant integrated with a novel split-flow configuration post-combustion CO₂ capture process. *Int J Greenh Gas Control* 2014;27:103–19.
- [13] Oko E, Wang M, Olaleye AK. Simplification of detailed rate-based model of post-combustion CO₂ capture for full chain CCS integration studies. *Fuel* 2015;142:87–93.
- [14] Peng J, Edgar TF, Eldridge RB. Dynamic rate-based and equilibrium models for a packed reactive distillation column. *Chem Eng Sci* 2003;58:2671–80.
- [15] Dunia R, Rochelle GT, Qin SJ. Subspace system identification for CO₂ recovery processes. *Proc. IEEE Int. Symp. Comput. Control Syst. Des.*, Department of Chemical Engineering, University of Texas, Austin, TX 78712, United States Department of Chemical Engineering and Material Sciences, University of Southern California, CA 90089, United States: 2011, p. 846–51.
- [16] Nittaya T, Douglas PL, Croiset E, Ricardez-Sandoval LA. Dynamic Modelling and Controllability Studies of a Commercial-scale MEA Absorption Processes for CO₂ Capture from Coal-fired Power Plants. *12th Int Conf Greenh Gas Control Technol GHGT-12* 2014;63:1595–600.
- [17] He Z, Sahraei MH, Ricardez-Sandoval LA. Flexible operation and simultaneous scheduling and control of a CO₂ capture plant using model predictive control. *Int J Greenh Gas Control* 2016;48:300–11.
- [18] Luu MT, Abdul Manaf N, Abbas A. Dynamic modelling and control strategies for flexible

operation of amine-based post-combustion CO₂ capture systems. *Int J Greenh Gas Control* 2015;39:377–89.

- [19] Hossein Sahraei M, Ricardez-Sandoval LA. Controllability and optimal scheduling of a CO₂ capture plant using model predictive control. *Int J Greenh Gas Control* 2014;30:58–71.
- [20] Mehleria ED, Mac Dowella N, Thornhillb NF. Model Predictive Control of Post-Combustion CO₂ Capture Process integrated with a gas-fired power plant. *PSE2015 ESCAPE25 n.d.:*27.
- [21] Abdul Manaf N, Cousins A, Feron P, Abbas A. Dynamic modelling, identification and preliminary control analysis of an amine-based post-combustion CO₂ capture pilot plant. *J Clean Prod* 2016;113:635–53.
- [22] Sipöcz N, Tobiesen FA, Assadi M. The use of Artificial Neural Network models for CO₂ capture plants. *Appl Energy* 2011;88:2368–76.
- [23] Li F, Zhang J, Oko E, Wang M. Modelling of a post-combustion CO₂ capture process using neural networks. *Fuel* 2015;151:156–63.
- [24] Li F, Zhang J, Oko E, Wang M. Modelling of a post-combustion CO₂ capture process using extreme learning machine. *Int J Coal Sci Technol* 2017;4:33–40.
- [25] Ayala Solares JR, Wei HL, Boynton RJ, Walker SN, Billings SA. Modeling and prediction of global magnetic disturbance in near-Earth space: A case study for Kp index using NARX models. *Sp Weather* 2016;14:899–916.
- [26] Roy RJ, Sherman J. A Learning Technique for Volterra Series Representation. *IEEE Trans Automat Contr* 1967;AC-12:761–4.
- [27] Fu FC, Farison JB. On the Volterra-series functional identification of non-linear discrete-time systems. *Int J Control* 1973;18:1281–9.
- [28] Bard Y, Lapidus L. Nonlinear System Identification. *Ind Eng Chem Fundam* 1970;9:628–33.
- [29] Schetzen M. Nonlinear System Modeling Based on the Wiener Theory. *Proc IEEE* 1981;69:1557–73. doi:10.1109/PROC.1981.12201.
- [30] Billings SA. Nonlinear system identification: NARMAX methods in the time, frequency, and spatio-temporal domains. 2013.
- [31] Leontaritis IJ, Billings SA. Input-output parametric models for non-linear systems Part I: Deterministic non-linear systems. *Int J Control* 1985;41:303–28.
- [32] Chen S, Billings SA. Extended model set, global data and threshold model identification of severely non-linear systems. *Int J Control* 1989;50:1897–923.
- [33] Wei HL, Billings SA, Liu J. Term and variable selection for non-linear system identification. *Int J Control* 2004;77:86–110. doi:10.1080/00207170310001639640.
- [34] Wei HL, Billings SA. Model structure selection using an integrated forward orthogonal search algorithm assisted by squared correlation and mutual information. *Int J Model Identif Control* 2008;3:341–56.
- [35] Dantas TSS, Franco IC, Fileti AMF, Da Silva F V. Nonlinear system identification of a refrigeration system. *Int J Air-Conditioning Refrig* 2016;24.
- [36] Gu Y, Wei H-L. Significant Indicators and Determinants of Happiness: Evidence from a UK Survey and Revealed by a Data-Driven Systems Modelling Approach. *Soc Sci* 2018;7:53.
- [37] Johansen TA, Brustad AF, Andersen TS, Kristiansen R. Nonlinear system identification of fixed wing UAV aerodynamics. *Proc. IASTED Int. Conf. Model. Identif. Control*, vol. 830, 2016, p. 44–51. doi:10.2316/P.2016.830-026.
- [38] Macedo MMG, Takimura CK, Lemos PA, Gutierrez MA. An automatic labeling bifurcation method for intracoronary optical coherence tomography images. *Prog. Biomed. Opt. Imaging - Proc. SPIE*, vol. 9417, 2015.

- [39] Billings SA, Korenberg MJ, Chen S. Identification of non-linear output-affine systems using an orthogonal least-squares algorithm. *Int J Syst Sci* 1988;19:1559–68.
- [40] Billings SA, Chen S, Korenbergs MJ. Identification of mimo non-linear systems using a forward-regression orthogonal estimator. *Int J Control* 1989;49:2157–89.
- [41] Zhu Y. *Multivariable system identification for process control*. Elsevier; 2001.
- [42] Wei HL, Billings SA. Improved model identification for non-linear systems using a random subsampling and multifold modelling (RSMM) approach. *Int J Control* 2009;82:27–42.